The *Moraxella* adhesin UspA1 binds to its human CEACAM1 receptor by a deformable trimeric coiled-coil

Rebecca Conners[1,4], Darryl J Hill[2,4], Elena Borodina[2], Christopher Agnew[1], Sarah J Daniell[2], Nicholas M Burton[1], Richard B Sessions[1], Anthony R Clarke[1], Lucy E Catto[1], Donna Lammie[3], Timothy Wess[3], R Leo Brady[1,*] and Mumtaz Virji[2,*]

[1]Department of Biochemistry, University of Bristol, Bristol, UK, [2]Department of Cellular and Molecular Medicine, University of Bristol, Bristol, UK and [3]Cardiff School of Optometry and Vision Sciences, Cardiff University, Cardiff, UK

Moraxella catarrhalis* is a ubiquitous human-specific bacterium commonly associated with upper and lower respiratory tract infections, including otitis media, sinusitis and chronic obstructive pulmonary disease. The bacterium uses an autotransporter protein UspA1 to target an important human cellular receptor carcinoembryonic antigen-related cell adhesion molecule 1 (CEACAM1). Using X-ray crystallography, we show that the CEACAM1 receptor-binding region of UspA1 unusually consists of an extended, rod-like left-handed trimeric coiled-coil. Mutagenesis and binding studies of UspA1 and the N-domain of CEACAM1 have been used to delineate the interacting surfaces between ligand and receptor and guide assembly of the complex. However, solution scattering, molecular modelling and electron microscopy analyses all indicate that significant bending of the UspA1 coiled-coil stalk also occurs. This explains how UspA1 can engage CEACAM1 at a site far distant from its head group, permitting closer proximity of the respective cell surfaces during infection.

*Corresponding authors. RL Brady, Department of Biochemistry, University of Bristol, University Walk, Bristol BS8 1TD, UK. Tel.: +44 117 331 2150; Fax: +44 117 331 2168; E-mail: L.Brady@bristol.ac.uk or M Virji, Department of Cellular and Molecular Medicine, University of Bristol, University Walk, Bristol BS8 1TD, UK. Tel. & Fax: +44 117 331 2035; E-mail: M.Virji@bristol.ac.uk
[4]These authors contributed equally to this work

Moraxella catarrhalis (*Mx*) is a human-specific bacterium present in the nasopharynx of up to 75% of healthy individuals, but frequently causes childhood otitis media, sinusitis and exacerbation of lung conditions in patients with chronic obstructive pulmonary disease (Karalus and Campagnari, 2000). As such, it is associated with widespread morbidity. However, there are no protective vaccines and antibiotic resistance is an increasing problem. Understanding the molecular events that facilitate the complex virulence mechanisms during *Mx* infection is key to the development of novel therapeutics and vaccines.

Infection by pathogenic bacteria such as *Moraxella* is initiated by multifunctional bacterial surface adhesin proteins that may additionally act in defensive roles to evade immune recognition (Karalus and Campagnari, 2000). A number of *Mx* adhesins have been identified and characterised from non-fimbriate (non-piliated) bacteria. These include the oligomeric coiled-coil adhesins (Oca, also recently classified as trimeric autotransporters; Linke *et al*, 2006) such as YadA from enteropathogenic *Yersinia enterocolitica*, Hia from *Haemophilus influenzae* (*Hi*) and the ubiquitous surface proteins UspA1 and UspA2 from *Mx*. A range of studies have confirmed the importance of these molecules in pathogenesis (Aebi *et al*, 1998; Lafontaine *et al*, 2000; Yeo *et al*, 2004; Attia *et al*, 2005; Heise and Dersch, 2006). The human carcinoembryonic antigen-related cell adhesion molecule 1 (CEACAM1), which is widely distributed on epithelial cells including those of the oropharynx and lower respiratory tracts (Hammarstrom, 1999), has been identified as a receptor for UspA1 (Hill and Virji, 2003). Other members of the CEACAM receptor family expressed on epithelia (CEA and CEACAM6) also bind to UspA1 (Hill *et al*, 2005), although these are less well studied. Over the past decade CEACAM1 has emerged as a common human receptor targeted by several respiratory pathogens (Virji *et al*, 1996; Hill *et al*, 2005). These include the opportunistic pathogens *Mx*, *Neisseria meningitidis* (*Nm*) and *Hi*, all of which interact with an overlapping site in the N-terminal domain of the receptor (N-CEACAM1) often leading to cellular invasion (Virji *et al*, 1999; Hill and Virji, 2003; Griffiths *et al*, 2007; Villullas *et al*, 2007). In addition, CEACAM1 is bound by strains of enterobacteria such as *Escherichia coli* and *Salmonella* (Leusch *et al*, 1991; Guignot *et al*, 2000) and several murine CEACAM1a isoforms serve as receptors for mouse hepatitis virus (Dveksler *et al*, 1993). A recombinant protein rD-7 (here referred to as UspA1[527–665]) based on this region of UspA1 has been shown to block binding of multiple respiratory pathogens, virtually eliminating binding of *Nm* and *Hi* isolates to human lung epithelial cells and substantially reducing *Mx* interactions (Hill *et al*, 2005). An antiadhesion strategy targeting N-CEACAM1 may therefore provide a unified

approach to control infections caused by these pathogens and an alternative to antibiotic treatment.

Electron microscopy studies have shown that YadA, UspA1 and UspA2 form dense forests of lollipop-like structures at the bacterial surface projecting from 200 Å (YadA) to 600–700 Å (UspA1) from the cell membrane (Hoiczyk *et al*, 2000). The UspAs have been shown by SDS–PAGE to form oligomeric structures (Cope *et al*, 1999). Amino-acid sequence comparisons have identified similar domains in YadA, Hia, UspA1 and UspA2 despite the considerable variations in their respective sizes (monomer masses are YadA 41–43 kDa, Hia 100–125 kDa, UspA1 88–100 kDa and UspA2 60–71 kDa). Each adhesin has a tripartite structure consisting of a head group, extended stalk region and membrane anchor domain. Although, up to now, no detailed structural information has been available for the UspAs, crystal structures have been reported for the head groups from YadA (Nummelin *et al*, 2004) and Hia (Yeo *et al*, 2004), the Hia membrane domain (Meng *et al*, 2006) and a theoretical model has been proposed for the overall structure of YadA (Koretke *et al*, 2006; Wollmann *et al*, 2006). In this model, the stalk has been proposed to adopt a trimeric coiled-coil structure with the C-terminal membrane anchor domain based on the crystal structure of a bacterial autotransporter (Oomen *et al*, 2004). This model has been supported by the crystal structure of the Hia membrane domain, which is constructed from four β-strands contributed from each of three monomers; the resulting 12-stranded β-barrel ensures trimerisation of the structure. Amino-acid sequence comparisons indicate that the UspAs differ most significantly from YadA in the length of both their head groups and stalk regions, and in the periodicity and handedness of the proposed coiled-coil (Hoiczyk *et al*, 2000).

UspA adhesins are multi-functional proteins for which a range of binding functions have been reported (see schematic in Figure 1). These include binding sites for fibronectin (Tan *et al*, 2005) and laminin (Tan *et al*, 2006), both in the N-terminal end of the UspAs where they are likely to be furthermost from the bacterial membrane and therefore most readily available for attachment. Serum resistance is also associated with UspA proteins as UspA2 contains a complement C3-binding region (regions 200–458) (Aebi *et al*, 1998) and both UspA1 and UspA2 bind to the complement binding protein C4bp (Nordstrom *et al*, 2004). Importantly, UspA1 has been shown to include a critical binding site for CEACAM1 away from the head group within residues 527–667 of the MX2 strain (Hill *et al*, 2005). In the extended 600- to 700-Å-long structure expected for UspA1 based on the YadA model (Koretke *et al*, 2006) this is expected to be at least 400 Å from the head group (see Figure 1). In contrast, the predicted four immunoglobulin superfamily extracellular domains of CEACAM1 could project only just over 100 Å from the epithelial cell surface. Matching of these regions and sufficiently close approach of the bacterial and host cell membranes to allow adhesion and infection to proceed would therefore appear difficult. In view of this apparent disparity and to explore the crucial importance of the UspA1–CEACAM1 interaction to *Mx* pathogenicity, in this study we have initially determined the structure of the CEACAM1 receptor-binding site in UspA1. This has then been combined with the crystal structure of N-CEACAM1 (Fedarovich *et al*, 2006) to reveal the structure of the CEACAM1:UspA1
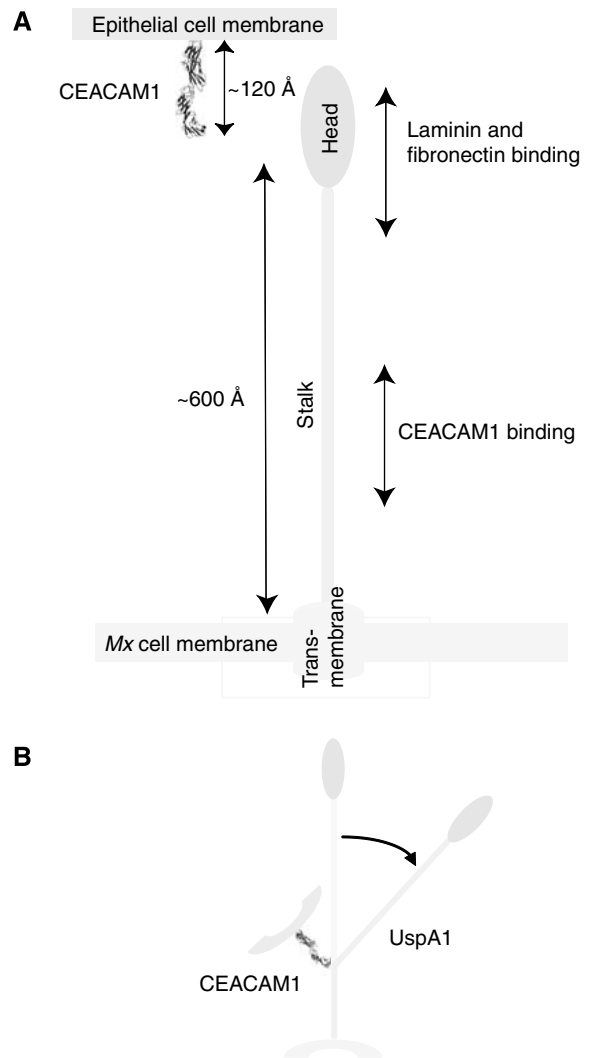

Figure 1 Schematic of UspA1. (**A**) The arrangement of proposed domains in UspA1 with the approximate regions of the binding sites for CEACAM1, laminin and fibronectin is shown. The latter two are located in the N-terminal region (UspA1 residues 299–452 and UspA2 165–318 for fibronectin (Tan *et al*, 2005), and UspA1 299–452 and UspA2 30–177 for laminin (Tan *et al*, 2006)), and by analogy with YadA (Nummelin *et al*, 2004) are likely to be within the head group. The bacterial cell membrane is at the bottom of the schematic. CEACAM1 is shown approximately to scale (represented here by the crystal structure of similarly sized CD4; Wu *et al*, 1997) bound to an epithelial cell membrane (top left). (**B**) Proposed model for bending of UspA1 in association with binding of CEACAM1 to allow adhesion and infection, as supported by the current study.

complex, assembled using a complementary approach combining data from crystallographic, mutagenesis and small-angle X-ray scattering (SAXS) techniques.

Results

The UspA1 CEACAM1-binding site is part of an extended trimeric coiled-coil

Initially, to probe the structural basis of the bacterial ligand–host receptor interaction, we determined the crystallographic structure of the $UspA1^{(527-665)}$ fragment. Although this region incorporates several regions with predicted low propensity for coiled-coil formation (Hoiczyk *et al*, 2000), $UspA1^{(527-665)}$

was found to form a contiguous, extended coiled-coil structure within the crystal lattice (Figure 2). Whereas earlier estimates of UspA1 oligomer composition were ambiguous, the crystal structure confirms that three polypeptide strands coalesce to form a left-handed trimeric coiled-coil. In each chain, there is clear electron density for 135 of the 139 amino acids with four residues (527–530) being disordered at the N terminus of each chain (this and all subsequent sequence numbering refers to UspA1 from the *M. catarrhalis* MX2 strain). As the trimer lies along the crystallographic three-fold axis, the conformation of each monomer within the trimer is identical. There are two monomers within the asymmetric unit and both are highly similar (root mean square deviation of all equivalent Cα's = 1.3 Å). The resulting rod-like structure is approximately 200 Å long and 20 Å in diameter.

To our knowledge, UspA1$^{(527-665)}$ forms the longest segment of triple coiled-coil for which a high-resolution structure has been determined. Overall, the average periodicity of the coil is 3.5 residues per turn with a pitch of about 150 Å, close to the expected hypothetical geometry (Lupas, 1996). Analysis of the structure with the coiled-coil software *SOCKET* (Walshaw and Woolfson, 2001) identified 84 'knobs into holes' interactions; all are of type 4 with packing

angles of between 45 and 60° as commonly observed in trimers. Although UspA1$^{(527-665)}$ appears to adopt a classic trimeric coiled-coil structure, there are a number of surprises. Whereas most of the internal hydrophobic residues (positions *a* and *d* by the standard convention; Lupas, 1996) are a mixture of alanines, isoleucines, valines and asparagines—as expected for trimeric coiled-coils—this pattern is disrupted at residue 573 when, unusually, a histidine is incorporated at a *d* position within the core. This is seen again three turns later at histidine 584 (position *a*) and then further after another 12 turns at histidine 629 (position *d*). For both histidines 584 and 629, the potential charge these residues incorporate within the core appears to be ameliorated through the incorporation of a bound phosphate ion. These ions are located equidistant (3.0 Å) from the histidine of each monomer (Figure 2B and C). The histidine rings are partially orientated through formation of a bifurcated hydrogen bond between each phosphate oxygen, a bound water, the main chain carbonyl group of Leu 580 (at His 584) and interactions with the neighbouring side chain of Ser 630 (at His 629). It is not clear whether binding of these phosphate ions, presumably from the crystallisation buffer, is biologically relevant.

We also observe density consistent with eight chloride ions bound within the central core of the coiled-coil (Figure 2D).
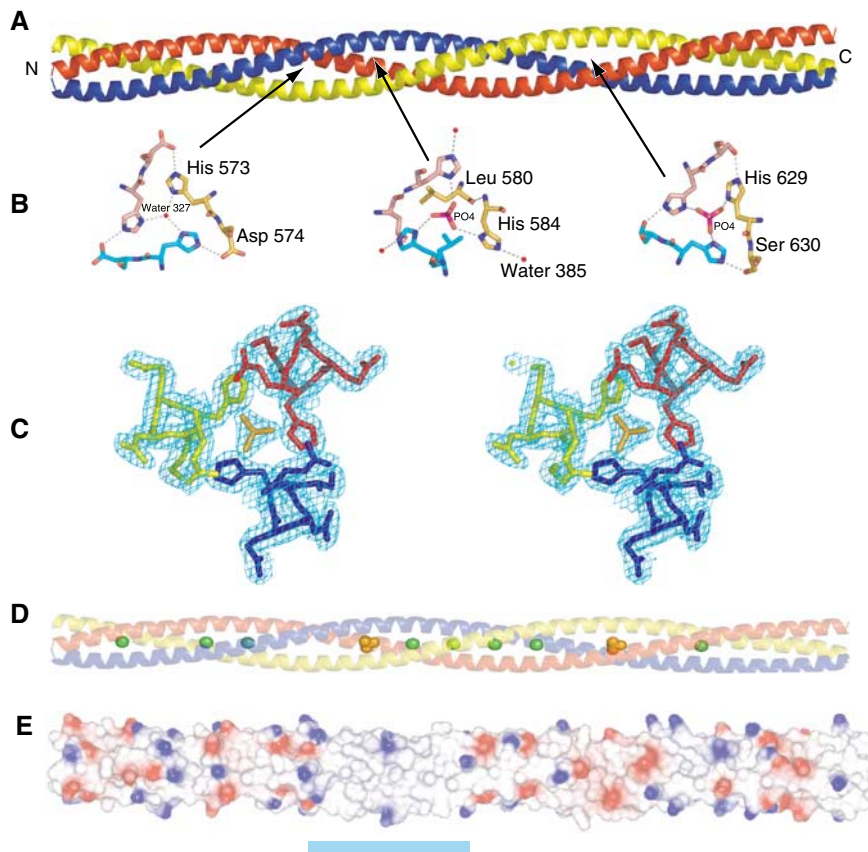

Figure 2 The crystal structure of UspA1$^{(527-665)}$. (**A**) Crystal structure of UspA1$^{(527-665)}$ shown as a Cα ribbon trace with chain A in yellow, chain B in red and chain C in blue. The amino terminus (N) of each chain is on the left, and carboxy terminus (C) on the right. (**B**) Hydrogen bonding interactions for the three internal histidine residues. Chain A in orange, chain B in pink and chain C in cyan. Their approximate location in the overall structure is indicated by the arrows. (**C**) Stereo view for representative electron density ($2F_{obs}-F_{calc}$, contoured at 1σ) corresponding to the buried His 629 region. (**D**) Locations of internally bound phosphate (orange) and chloride (green) ions within the central coiled-coil cavity. (**E**) Overall electrostatic surface of UspA1$^{(527-665)}$. The hydrophobic patch proposed to be the receptor-binding site is indicated by the blue bar. The scale and orientation of UspA1$^{(527-665)}$ is the same throughout (A, D, E).

These are present when an asparagine residue is encountered in the central cavity of the coiled-coil (position *d*), and in each instance the ions interact via the amide nitrogen of the asparagine side chain with distances ranging from 3.1 to 3.2 Å. Chloride ions have been observed previously in the central core of a number of similar structures including those of fibritin (Tao *et al*, 1997) and the spike glycoprotein from the SARS coronavirus (Duquerroy *et al*, 2005) and are proposed to add specificity in aligning the individual monomers of the coiled-coil.

Finally, the degree of helical supercoiling relaxes towards the C terminus where there is a stutter in the sequence starting from Ser 657 (three residues of the heptad appear to be missing) and a decrease in supercoiling is evident. Because of the breakdown in the pattern of core hydrophobic residues, this distortion is likely to be inherent within the sequence rather than a response to the artificial truncation of the coiled-coil within this recombinant construct.

Stability of the coiled-coil stalk

The unexpected incorporation of potentially charged histidine side chains within the hydrophobic core of the trimeric assembly led us to speculate that protonation of these groups might provide a mechanism for destabilisation of the assembly, hence potentially initiating or assisting flexibility within the rod-like structure. Circular dichroism (CD) was used to assay the helical content of UspA1$^{(527-665)}$ in response to changes in pH (Figure 3). These data indicated a sharp transition from a helical folded structure (assumed to be coiled-coil) to random coil once the pH dropped below 4.8. Protonation of the histidine side chains (normally expected to occur at pH 6, but often reduced in hydrophobic core regions), introducing repulsive positive charges within the core of the trimer, would be expected to be incompatible with trimer assembly. However, these data also confirm that the coiled-coil form must prevail at physiological pH.

UspA1$^{(527-665)}$ forms a stable complex with N-CEACAM1

Next, we used gel permeation chromatography (GPC), analytical ultracentrifugation (AUC) equilibrium sedimentation studies (Figure 4) and isothermal calorimetry (ITC) to confirm that N-CEACAM1 forms a stable complex in solution with UspA1$^{(527-665)}$. In all cases, self-aggregation and the extended shape of UspA1$^{(527-665)}$ lead to non-ideal behaviour, complicating the data interpretation. On GPC, UspA1$^{(527-665)}$ runs anomalously, eluting with an apparent molecular mass of 110 kDa (expected mass of trimer 45 494), whereas N-CEACAM1 (expected mass 11 747) appeared to be 19.5 kDa, perhaps reflecting its known propensity for homo-dimerisation (Watt *et al*, 2001) (Figure 4A). The complex of UspA1$^{(527-665)}$ with N-CEACAM1 eluted with an apparent molecular mass of 150 kDa; this peak broadening on the addition of excess N-CEACAM1. Similarly, global fit analysis of sedimentation equilibrium AUC data (Figure 4B) indicated a mass of 27 237 for N-CEACAM1 suggesting a dimer, and a mass of 43 896 for UspA1$^{(527-665)}$ indicative of a trimer. Determination of the mass of their complex was complicated by pronounced pressure effects (Kegeles *et al*, 1967) that lead to a reduction in observed apparent mass at higher speeds. Global fit analysis of the lower speed data for the complex gave a mass of 74 162, which appears consistent with one UspA1$^{(527-665)}$ trimer binding either one N-CEACAM1 dimer
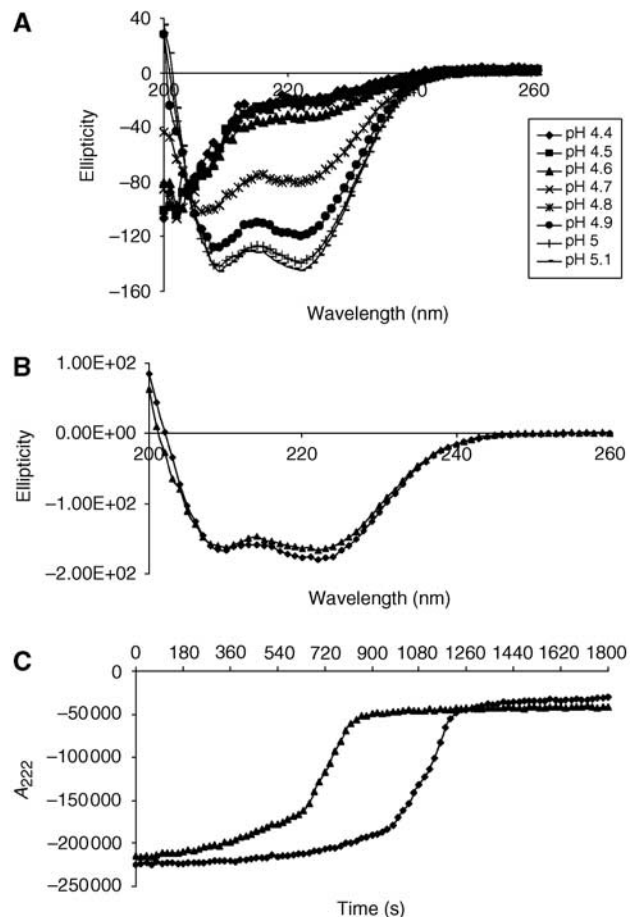

Figure 3 Circular dichroism (CD) spectra. (**A**) CD spectra from UspA1$^{(527-665)}$ across a range of pH values. (**B**) CD spectra of native UspA1$^{(527-665)}$ (solid diamonds) compared with the M586A/A588Q mutant (solid triangles). (**C**) Melting curves for native (solid diamonds) and the mutant (solid triangles) proteins measured by monitoring absorbance at 222 nm against increasing time and temperature (2°C increases in temperature every 180 s from 29 to 47°C). All spectra were obtained at room temperature at 0.1 mg/ml in 50 mM phosphate-acetate buffer using a Jobin-Yvon CD6 spectropolarimeter, and are an average of at least two scans after substraction of the spectra of the buffer.

or two monomers, although lower masses were obtained from the higher speed data. Aggregation of UspA1$^{(527-665)}$ and competing homo-dimerisation of N-CEACAM1 (Watt *et al*, 2001) also affected the quality of the ITC data (Figure 4C). However, these data confirm each trimer of UspA1$^{(527-665)}$ can readily bind up to two molecules of N-CEACAM1 ($N = 2.0 \pm 0.2$) with high affinity (estimated K_D 24 ± 22 nM), after which only weak, possibly nonspecific, further association is observed. Taking into account the limitations of each of these techniques in analysing this complex association event, in summary we concluded that each trimer of UspA1$^{(527-665)}$ provides a high-affinity binding site for a maximum of two molecules of N-CEACAM1.

Location of the receptor-binding site on UspA1

An electrostatic potential surface calculated from the UspA1$^{(527-665)}$ crystal structure (Figure 2E) displayed a predominance of anionic and cationic regions on the solvent-accessible coiled-coil surface. However, one section of the coiled-coil was striking for its deviation from this pattern. The
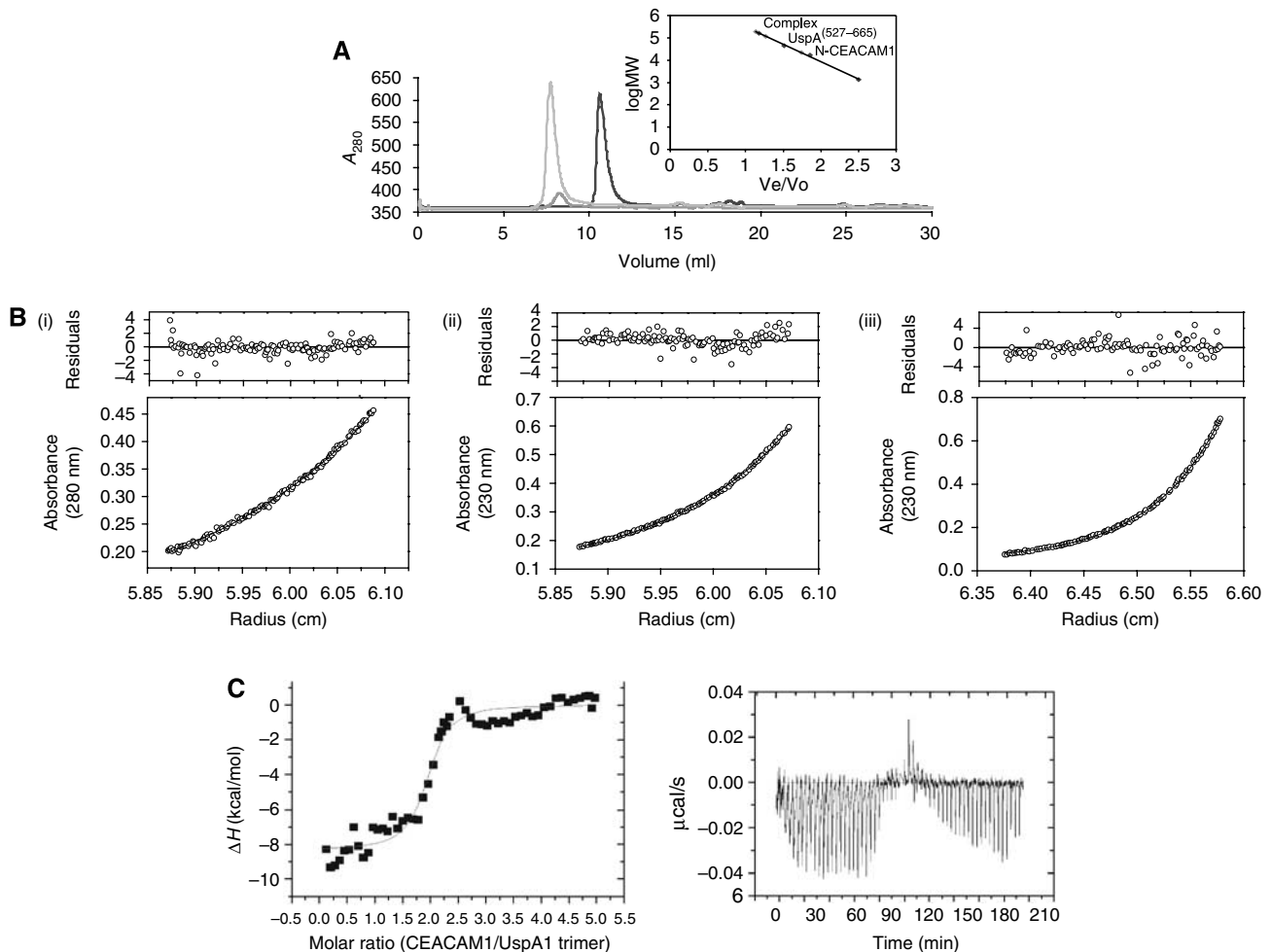
Figure 4 Formation of the UspA1$^{(527–665)}$/N-CEACAM1 complex. (**A**) GPC analysis. Samples of N-CEACAM1 (blue, right), UspA1$^{(527–665)}$ (red, middle) and N-CEACAM1/UspA1$^{(527–665)}$ complex (green, left) were run individually on an XK16/60 Superdex 75 column in 50 mM Na Hepes, pH 8.0 and 150 mM NaCl. The complex was formed by incubating amounts equivalent to one UspA1$^{(527–665)}$ trimer to one N-CEACAM1 dimer at 18°C for 16 h. UspA1$^{(527–665)}$ absorbs poorly at 280 nm due to the absence of tyrosine and tryptophan resides. (**B**) AUC sedimentation equilibrium analysis. The main panels show the absorbance for (i) N-CEACAM1, (ii) UspA1$^{(527–665)}$ and (iii) complex, as a function of the radius of centrifugation, following centrifugation at 20°C for 24 h at 16 000 r.p.m. The absorbance was recorded at 280 nm in (i) and at 230 nm in (ii) and (iii). In each case, the fitted line corresponds to a global fit to M in Equation (1) of reference (Murphy *et al*, 2006) for multiple datasets at a range of speeds (see Materials and methods). The best fit was obtained with an M for (i) 27 237 ± 976; for (ii) 43 896 ± 590 and (iii) 74 162 ± 912. The upper panels show the distribution of the residuals between the data and the fit. (**C**) ITC analysis. Isothermal titration of UspA1$^{(527–665)}$ with N-CEACAM1 shows an initial strong binding event ($K_D = 35$ nM, $N = 2$) followed by apparent weak association events that may result from the weaker ligand dimerisation. The inset shows raw titration data. A full-colour version of this figure is available at the *The EMBO Journal Online*.

segment 578–597 contains only one charged residue—histidine 584—which is buried within the hydrophobic core (see above). The exterior surface of this segment is notably hydrophobic (white in Figure 2E). This region is located just over one-third of the way along the rod-like structure, approximately 80 Å from the N terminus.

As this distinctive patch also overlapped with a normally highly conserved region, which is unusually absent in the UspA1 of *Mx* O35E strain that does not bind to N-CEACAM1 (Supplementary data), site-directed mutants of surface residues both within and adjacent to this region were prepared. Each of the mutants was selected and designed to have minimal impact on the coiled-coil formation. The mutants made are shown in Figure 5A and include changes to amino acids expected to be exposed at the binding interface (L583A, M586A, A588Q and A590Q), a double mutation (M586A/A588Q) and a control substitution (A568Q) from outside the

predicted region of the N-CEACAM1 interaction. Western blotting was used to confirm that in each case the purified mutant protein retained the ability to form trimers indicative of retention of the coiled-coil structure (Supplementary data). This was further confirmed for the double mutant (M586A/A588Q) where the CD spectra of both the native and mutant proteins were found to be essentially identical (Figure 3B) and only a minor thermodynamic difference was observed in their melting temperatures (41 and 39°C, respectively; Figure 3C). These observations confirm that the amino-acid substitutions introduced do not affect the structure or assembly of the coiled-coil, indicating that altered binding effects are likely to arise from direct contacts of these amino acids with N-CEACAM1 rather than by disruption of the UspA1 gross structure.

The ability of these mutant UspA1$^{(527–665)}$ proteins to bind CEACAM1-Fc was measured in an ELISA and is summarised
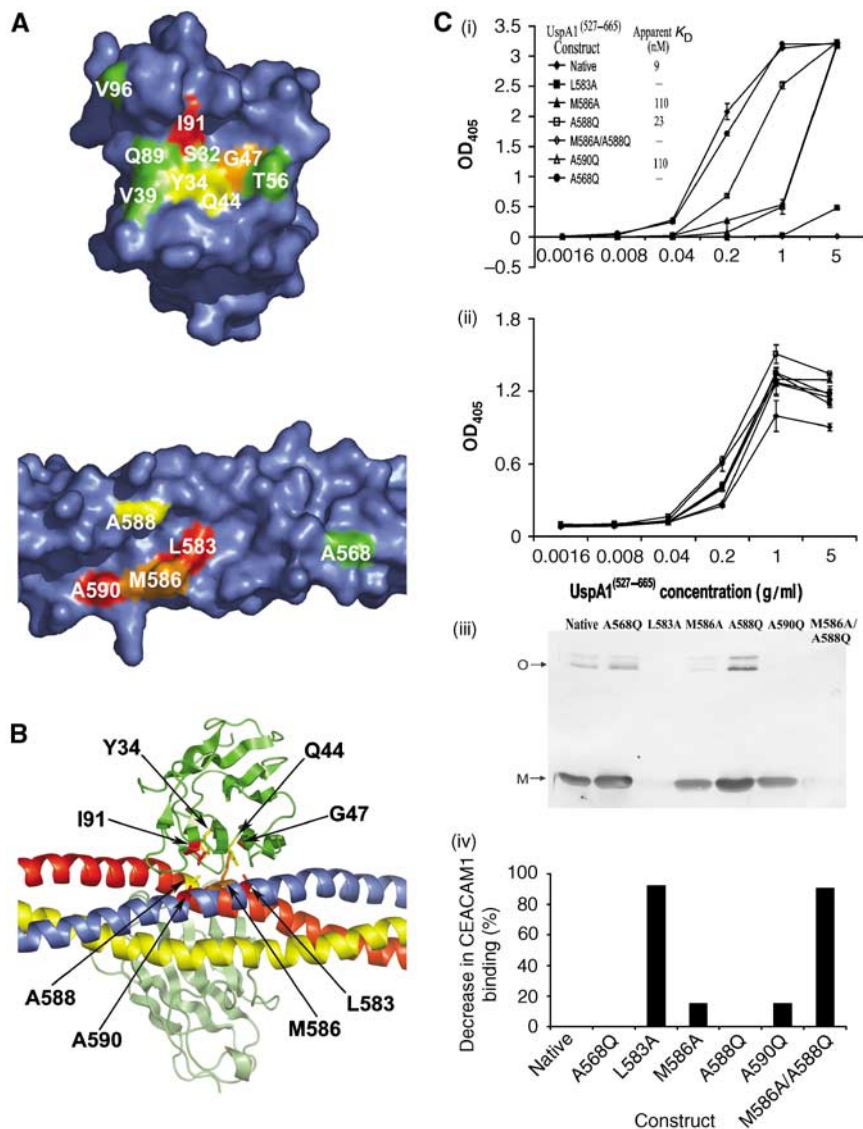
Figure 5 Site-directed mutagenesis and UspA1$^{(527–665)}$/CEACAM1 binding. (**A**) Location of residues shown to affect binding on the surface of the crystal structures shown after opening of the model interface for the complex (rotated 180° around an axis across the page) for UspA1$^{(527–665)}$ (bottom) and for N-CEACAM1 (top). Mutated residues generating a large reduction in binding are shown in red, medium in orange, moderate in yellow and no effect in green. (**B**) Location of the interface residues in the model of the assembled complex. UspA1 is coloured as in Figure 2, and the N-CEACAM1 molecules in green. (**C**) Effect of UspA1$^{(527–665)}$ amino-acid substitutions on CEACAM1-Fc binding. (i) ELISA: microwells coated with UspA1$^{(527–665)}$ constructs at concentrations shown and binding was assessed using receptor at 0.5 μg/ml. Apparent K_D values calculated where possible are also shown. (ii) The constructs were overlaid with anti-polyhistidine antibody to indicate the amounts that are present in the assay. Data shown $n = 4 \pm$ s.e. (iii) Western blot of UspA1$^{(527–665)}$ constructs as indicated overlaid with CEACAM1-Fc (0.5 μg/ml) corroborates the ELISA data. CEACAM1 bound both the monomers (M) and the oligomers (O) of the UspA1$^{(527–665)}$ constructs. The relative CEACAM1 binding in (iii) determined by densitometric analysis is shown in (iv).

in Figure 5B. No significant difference in binding was observed between the wild-type UspA1$^{(527–665)}$ and the control construct (A568Q) at any of the concentrations tested. At limiting CEACAM1 concentration, decreased CEACAM1 binding was observed at one or more UspA1 concentrations for all of the other constructs. The most striking effect on CEACAM binding was observed for the mutants L583A, M586A, A590Q and the double substitution (M586A/A588Q) (Figure 5B). Comparable binding of anti-polyhistidine antibody was observed to all constructs confirming equivalent coating of all constructs to the ELISA plate (Figure 5C, ii). These studies indicated that the order of importance of single UspA1 residues involved in CEACAM1 engagement appears to be L583 > A590 > M586 > A588.

These binding data were also supported by western blotting analysis in which UspA1$^{(527–665)}$ constructs were overlaid with CEACAM1-Fc and detected by an anti-Fc antibody (Figure 5C). In these assays, no decrease in binding was evident between native UspA1$^{(527–665)}$, the A568Q control or the A588Q substitution. A decrease in CEACAM1 binding was observed to M586A (14.8%), A590Q (15.0%), L583A (92.0%) and the double substitution (90.4%). These data parallel the ELISA data and affirm the relative importance of UspA1 residues involved in CEACAM1 engagement as L583 > A590 > M586 > A588. It is interesting to note that in both ELISA studies and western blot analysis the double substitution M586A/A588Q abrogates binding and this appears to be a synergistic effect in both techniques. Such

data highlight the importance of multiple amino-acid engagement in the interaction of UspA1 and CEACAM1.

The UspA1-binding site on its CEACAM1 receptor

Identification of the surface on CEACAM1 that interacts with UspA1 was facilitated by a number of prior observations: (1) other pathogens—*Nm* and *Hi*—that recognise N-CEACAM1 have been found to use a site centred on the critical CEACAM1 residue I91 (Virji *et al*, 1999; Villullas *et al*, 2007); (2) this site also forms an epitope for an anti-CEACAM1 antibody shown to block binding of *Nm* and *Hi* as well as *Mx* (Hill and Virji, 2003); (3) recombinant UspA1[(527–665)] inhibits binding of all three pathogens to CEACAM1(Hill *et al*, 2005). Combining these earlier results, we surmised that the UspA1-binding site must at least partially overlap with the site also used by *Nm* and *Hi*. We therefore mutated I91 and surrounding residues on CEACAM1 to define the extent of the UspA1-binding site. In ELISA studies, binding of N-CEACAM1 to UspA1[(527–665)] was significantly impaired when I91 was mutated to Ala, and moderate reductions in binding accompanied mutation of surrounding residues Y34, Q44 and G47, whereas little or no effect was noted for the mutations of S32, T56, V39, V96 and Q89 (Figure 5A and Supplementary data). No reduction in binding was also noted for V39A, confirming UspA1 binds to the monomeric form of CEACAM1 as this mutation has previously been shown to abolish dimerisation (Watt *et al*, 2001). Interestingly, the introduction of a leucine side chain to CEACAM1 position 56 partially restored binding to the UspA1 L583A mutant. From our model of the complex (see below) it was anticipated that these mutations should be compensatory.

In summary, the mutagenesis data for both UspA1[(527–665)] and N-CEACAM1 when combined with their respective crystal structures enabled us to locate their interacting surfaces.

The N-CEACAM1:UspA1[(527–665)] complex

A tentative model for the complex of N-CEACAM1 with UspA1[(527–665)] was then prepared by assembling the two individual crystal structures. This preliminary model was built by comparing the respective sites identified by site-directed mutagenesis, manually assembling the two surfaces in the most complementary orientation (Figure 5A) followed by energy minimisation of the complex. This generated an interface in which the UspA1 residues M586 and A590 are in close proximity to I91 of the receptor, UspA1 A588 is adjacent to Y34, V39 and Q89 of CEACAM1 and UspA1 L583 lies next to Q44, G47 and T56 of CEACAM1. These residues form the region identified by the mutagenesis studies to affect binding. The complementary nature of these surfaces was only marred by a small protrusion of the F/G loop of N-CEACAM1, a region that is involved in a homo-dimerisation interaction around a two-fold axis in the crystal structure (Fedarovich *et al*, 2006). It is likely that this conformation is not maintained within the monomeric form of N-CEACAM1 which, as confirmed by the binding of the monomeric V39A mutant (Watt *et al*, 2001), is the active form for binding to UspA1 (Supplementary data). Although the actual conformation of the F/G loop in this form is uncertain, we noted that on energy minimisation of the complex this region protrudes into a distinctive cavity formed at the interface (Figure 5A), possibly assisting partial unwinding of the coiled-coil
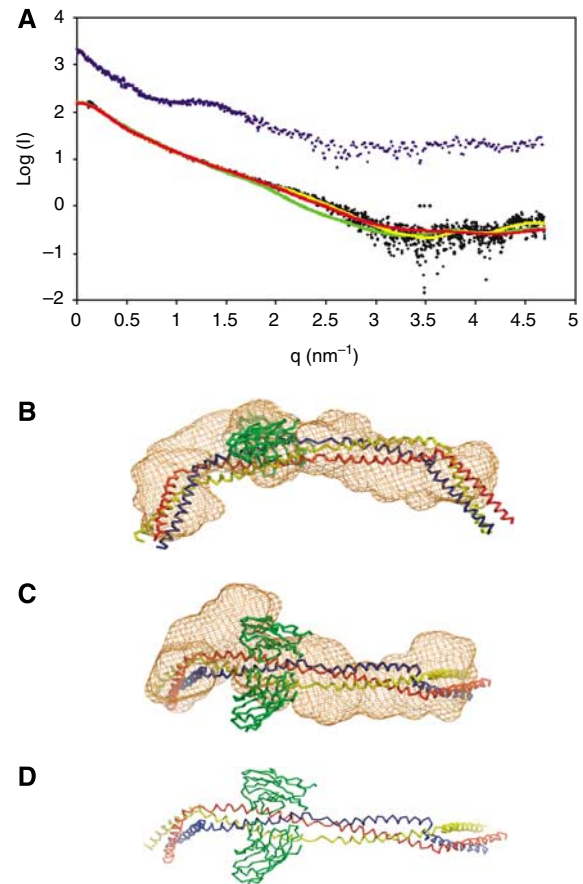
Figure 6 Solution structure of the UspA1[(527–665)]/CEACAM1 complex. (**A**) Experimental SAXS scattering curve (black dots) for UspA1[(527–665)]/CEACAM1 complex overlaid with the fits of the envelope (yellow), bent (red) and straight (green) complex models shown below. The scattering data for unliganded UspA1[(527–665)] is shown as blue dots. (**B**, **C**) Two orthogonal views of the bent complex model (coloured as in Figure 5) superimposed on this envelope, which is the median reconstruction selected by DAMAVER are shown (Volkov and Svergun, 2003). (**D**) The same model without the envelope is shown.

assembly. The surface area occupied by the N-CEACAM1 molecule is approximately one-third of the circumferential surface area in the proposed binding site region of the UspA1 trimeric structure, implying that three N-CEACAM1 molecules could bind simultaneously. This is in contrast to the AUC and ITC data (Figure 4) which show that, in practice, only two N-CEACAM1 molecules bind with high affinity to UspA1[(527–665)].

Binding of receptor correlates with bending of the stalk region of UspA1

To validate the proposed model for the N-CEACAM1/UspA1[(527–665)] complex, we obtained SAXS data. The scattering patterns of solutions of the complex and of uncomplexed UspA1[(527–665)] are presented in Figure 6A. There is further indication of the self-aggregation behaviour also noted at high concentrations of uncomplexed UspA1[(527–665)] in the AUC studies, and this prevented reliable interpretation of the SAXS data from the unliganded form. However, the scattering curve changes upon complex formation of UspA1[(527–665)] with N-CEACAM1, and is consistent with a mono-disperse

solution with an estimated molecular mass that agrees well with the value predicted from the primary sequence of the expected complex. The distance distribution function $p(r)$ of the complex suggests an elongated shape with a maximum diameter of ~ 14 nm and a cross section of ~ 2 nm (the latter parameter corresponds to a maximal $p(r)$). The experimental radius of gyration was 4.58 ± 0.09 nm.

A low-resolution model of the complex was reconstructed *ab initio* from the experimental scattering patterns. Reconstructions using DAMMIN (Svergun, 1999) yielded similar envelopes with consistently reasonable fits to the experimental data (χ values of ~ 1.5) and which could be readily superimposed (mean NSD (Volkov and Svergun, 2003) of 0.88) (Figure 6). Although the data indicate a diversity of potential fits, all of the shapes share the same essential features: the complex is seen to be elongated and is of comparable dimensions (approximately 200 Å in total length, 20–30 Å in diameter) to the UspA1 crystal structure. Distinctively, however, there is a significant bend in the molecule (30–60° deflection from the linear form in the various models), resulting in a 'boomerang' shape. Adjacent to the apex of this bend there is a thickening of the envelope, approximately sufficient to accommodate two N-CEACAM1 domains. Bending of the UspA1 rod was approximated by splitting the modelled complex into four equal lengths. These were fitted to the scattering data as separate rigid bodies using the software SASREF (Petoukhov and Svergun, 2005). A complete model of the complex was generated by rejoining of the UspA1 polypeptide chains followed by energy minimisation. This model was then fitted to the scattering data using the software CRYSOL (Svergun *et al*, 1995), which resulted in a χ value of 1.45. By contrast, attempts to fit the predicted scattering from a complex in which UspA1[(527–665)] retained a straight rod-like shape produced significantly poorer correlation with the experimental data (χ value of 3.11; Figure 6A).

To explore the feasibility of this model of the complex, molecular dynamics simulations were undertaken (Supplementary data). Simulations of the unliganded form of UspA1[(527–665)] indicated this form, although showing some flexibility, remained fully extended across the period of the simulation. In contrast, the same simulations conducted in the presence of one or two bound N-CEACAM1s and commencing with the straight form of UspA1[(527–665)] reproducibly showed distinctive bending was induced. This distortion rapidly led to distortions of 30–70°, similar to those observed in the SAXS envelopes.

By inference, this distorted model for the complex is also supported by the observation from both the AUC and ITC studies that only two molecules of N-CEACAM1 can bind each initially symmetrical trimer of UspA1. The absence of strong binding to the third site implies distortion of this remaining site, and hence of the UspA1 molecule. Finally, using transmission electron microscopy (Supplementary data), we have also observed that UspA1 appears to adopt not only extended structures in the surface array of *Mx* but significant perturbations also appear to be more prevalent in the presence of CEACAM1 receptor. Through gene deletions (Hoiczyk *et al*, 2000) it has previously been established that the most extended molecules at the *Mx* surface predominantly comprise UspA1. This demonstrates that both linear and distorted conformations of UspA1 are possible on the

bacterial surface (Supplementary data). Although the resolution in these studies is insufficient to correlate the shapes observed directly with the structural model of the complex presented herein, these changes are consistent with the SAXS observations, and molecular dynamics simulations.

Discussion

Coiled-coil motifs have been increasingly identified within a wide range of proteins and are believed to perform a variety of roles delivered by extended, relatively rigid structures (reviewed in Lupas, 1996). Although many coiled-coil proteins are dimeric, parallel trimeric coiled-coil structures have been reported for a number of viral and bacterial proteins, including the influenza hemagglutinin (Wilson *et al*, 1981; Bullough *et al*, 1994), murine leukaemia virus spike protein (Fass *et al*, 1996), mannose-binding protein (Sheriff *et al*, 1994) and in the stalk of the head group of the UspA1-related protein YadA (Nummelin *et al*, 2004). In all of these cases, the trimeric structure acts as a stalk to project other bio-active domains away from the pathogen membrane. In none of these cases, however, does the coiled-coil region itself act as ligand, instead playing a supporting structural role. The partial structure of UspA1 reported in this study is different. First, at about 200 Å in length (double the extended hemagglutinin structure), UspA1[(527–665)] represents the longest stretch of trimeric coiled-coil for which a detailed structure is available. Second, UspA1 is unusual in utilising an extended stretch of regular coiled-coil as a receptor-binding domain. This is the first definitive example of this function for a trimeric coiled-coil, but it is likely there are others. For example, the M-like fibrinogen (Fg)-binding protein from the equine-specific bacterium *Streptococcus equi* has also previously been reported to contain an Fc-receptor-binding region within a multimeric coiled-coil stalk (Meehan *et al*, 2002), although no structural details are available.

The UspA1 protein is present at high density on the bacterial cell surface, and electron microscopy studies (Hoiczyk *et al* (2000) and Supplementary data) indicate this leads to forest-like densities in which the head groups may limit access to the closely packed stalk (trunk) regions. This arrangement is consistent with the linear structure observed for the uncomplexed form of UspA1[(527–665)] within the crystal lattice; maximisation of crystal contacts would be expected to favour this form. At the bacterial surface, close packing of adhesins might be encouraged by the hydrophobic nature of the ligand-binding site and may, through restricting access of large antibodies, confer some protection of this region from immune recognition. This arrangement, however, presents a problem in that the resulting physical locations of the respective ligand/receptor pair seem incongruous to permit sufficiently close approach of bacterial and human cell membranes to allow effective adherence via the CEACAM1-binding site. Electron microscopy studies indicate UspA1 extends approximately 600–700 Å from the bacterial cell surface (Hoiczyk *et al*, 2000). This is consistent with the expected length of an extended coiled-coil segment (residues 333–742) of which UspA1[(527–665)] represents approximately one-third (200 Å). In the fully extended intact ligand, the receptor-binding site would therefore be located at least 450 Å from the membrane-distal end of UspA1. In contrast, its receptor site on human CEACAM1—by analogy with its

similar construction to CD4 for which an overall structure is known (Wu *et al*, 1997)—can reach no further than about 120 Å from the epithelial cell surface. Even if the receptor is primarily located within the highly invaginated microvilli of epithelial cells (Hammarstrom, 1999) the sheer bulk created by the length of the extended head group would seem to present a steric difficulty for placing the ligand and receptor in close proximity. Two explanations seem possible. The head group of UspA1 may insert into the epithelial cell membrane prior to attachment of CEACAM1, allowing the base of the stalk region to come into closer proximity to epithelial cell surface. Alternatively, as suggested by this study, the stalk of UspA1 is capable of changing conformation to allow closer approach of the two respective membranes (Figure 1B).

Deformability of the UspA1 stalk region is demonstrated by the solution scattering studies, where in the presence of its CEACAM1 receptor UspA1$^{(527-665)}$ displays a distinctive curvature (bending angle of approximately 30–60°). This implies that in its receptor complex the UspA1 stalk has increased flexibility. Although self-aggregation prevents us from accurately interpreting similar solution scattering data collected in the absence of CEACAM1, the change in the scattering curve that accompanies addition of the receptor (Figure 6A) is consistent with an alteration in the molecular structure. Further, as the crystal structure shows UspA1$^{(527-665)}$ to be symmetrical there appears to be no inherent mechanism for it to adopt a discrete bend (an asymmetric structure) in the absence of other effectors. This is supported by the molecular dynamics simulations, which indicate that the extended structure exhibits a degree of flexibility, but remains rod-like overall. In contrast, the same simulations conducted in the presence of bound N-CEACAM1 reveal a 'weak spot' within the trimeric coiled-coil in the vicinity of residue 610, equidistant between the CEACAM1-binding site and the stutter and coincident with the incorporation of internally bound ions (Figures 2 and 6). Binding of N-CEACAM1, therefore, seems to provide a mechanism to 'break' the three-fold symmetry and hence encourage formation of the bowed structure. The asymmetry produced by the bending is likely to distort remaining binding sites generated by the inherent three-fold symmetry, accounting for the observation that a maximum of two N-CEACAM1 molecules readily associate with each UspA1 trimer. Binding of receptor may also disrupt interactions of this hydrophobic region with neighbouring copies of UspA1 (akin to disruption of aggregation in the SAXS studies). The observation of curvature of UspA1 when in complex with its receptor noted in the solution scattering studies is supported by (i) the molecular dynamics simulations; (ii) the electron microscopy studies of the *Mx* cell surface where significant perturbations of the adhesin 'forest' are observed and (iii) is a logical inference from the AUC and ITC measurements of a maximal stoichiometry of two molecules of N-CEACAM1 can bind with high affinity to each trimer of UspA1. In combination, these data support the concept of increased flexibility and the ability to adopt a distinctly bowed structure when UspA1$^{(527-665)}$ binds to its N-CEACAM1 receptor.

It is possible that this potential for the stalk region of UspA1 to bend within this discrete region may arise from the internal histidines and/or the stutter within the UspA1$^{(527-665)}$ coiled-coil, which appear unique to this part of UspA1. The CD unfolding data highlight the marked

Table I Summary of X-ray diffraction data and refined model statistics for UspA1$^{(527-665)}$

Diffraction data	
Resolution range (Å)	50–1.9 (1.97–1.9)
Space group	P3
Unit cell	$a = b = 37.23$, $c = 224.48$
	$\alpha = \beta = 90°$, $\gamma = 120°$
Completeness (%)	93.5 (69.9)
Total no unique reflections	27 647 (1963)
Redundancy	9.4 (3.5)
$I/\sigma I$	19.6 (2.1)
R_{sym} [a]	0.086 (0.400)
Wilson B factor	19.8
Refinement statistics	
Total no. of reflections	24 555 (1332)
No. of reflections in test set	1300
R_{cryst} [b]	0.194 (0.206)
R_{free}	0.253 (0.313)
RMSD: bond lengths (Å)	0.016
RMSD: bond angles (deg)	1.241
RMSD: bonded B factors––main chain	0.656
RMSD: bonded B factors––side chain	1.830
Protein atoms	2088
Solvent molecules	386
B-average, protein (Å^2)	21.7
Residues in most favoured regions, Ramachandran plot (%)	100

Values in parentheses are the statistics for the highest resolution shell.
[a]$R_{sym} = \Sigma_{hkl} \Sigma_I |I_i(hkl) - \langle I(hkl) \rangle| / \Sigma_{hkl} \Sigma_i I_i(hkl)$.
[b]$R_{cryst} = \Sigma_{hkl} |F_o(hkl) - F_c(hkl)| / \Sigma_h |F_o(hkl)|$.
Refined models were validated using Molprobity (Lovell *et al*, 2003).

instability of the coiled-coil structure to decreases in pH. Considering also the adjacent stutter, this whole region may be readily susceptible to the types of deformation seen in the SAXS analysis, molecular dynamics simulations and EM studies. By corollary, the extended triple coiled-coil in influenza hemagglutinin incorporates both buried histidines and several stutters along its length (Bullough *et al*, 1994) and is believed to be metastable—allowing a dramatic re-modelling to take place as the pH is changed. The stimulus that instigates the conformational change in UspA1—whether chemical or mechanical—is unknown. It is possible that the composition of this region simply makes it more susceptible to deformation in response to mechanical force. Electron microscopy studies of UspA1 (Hoiczyk *et al*, 2000 and Supplementary data) and the related protein EmaA (Ruiz *et al*, 2006) at their respective cell surfaces indicate that a variety of conformations are observed but distinctive kinks are evident in both cases. Bending may be initially required to allow access for the receptor, which then stabilises this conformation by breaking the three-fold symmetry of the UspA1 stalk.

A recent structural determination of the *E. coli* Dr adhesin bound to its human CEA receptor indicates that Dr also binds across the homo-dimer-forming surface of the receptor (Korotkova *et al*, 2008). This is very similar to the surface of CEACAM1 eclipsed by UspA1 in the current study (Korotkova *et al*, 2008). Note that the bacterium may achieve an advantage in targeting this largely invariant surface of the receptor. In both cases, it would be expected that adhesin binding would be accompanied by disruption of

the homo- and heterophilic interactions known to occur between members of the CEACAM family (Watt *et al*, 2001; Korotkova *et al*, 2008).

UspA1 is also known to interact with laminin (Tan *et al*, 2006), a component of the basement membrane, and with fibronectin (Tan *et al*, 2005), which is prevalent in the extracellular matrix. Both these activities have been localised to the head group or nearby region. It is not known whether UspA1 can bind these ligands simultaneously in addition to CEACAM1. Further studies are required to provide a composite model for the multi-functional behaviour of UspA1, including its dynamic responses to the mechanical forces encountered as the bacterium encounters its host cell. Finally, UspA1$^{(527-665)}$ has been shown to block binding of *Mx*, *Nm* and *Hi* clinical isolates and to generate a protective immune response against all *Mx* isolates tested (Hill *et al*, 2005). From the identification of the N-CEACAM1-binding site and its molecular structure provided by these studies, it may now be possible to engineer smaller constructs with valuable therapeutic applications.

Materials and methods

Bacterial strains

The *M. catarrhalis* strains MX2 ATCC 25238 and 035E were grown as described in previous studies (Hill and Virji, 2003; Hill *et al*, 2005).

Recombinant protein purification and ELISA

Expression and purification of UspA1$^{(527-665)}$ has been described previously (Hill *et al*, 2005). Refolded UspA1$^{(527-665)}$ was purified further by GPC on an XK16/60 Superdex 75 column (GE Healthcare) in 50 mM Tris, pH 8.0 and 150 mM NaCl. Recombinant N-CEACAM1 was prepared as described in Fedarovich *et al* (2006). Mutant UspA1$^{(527-665)}$, and N-CEACAM1 proteins were prepared as described in Supplementary data. The production of soluble CEACAM1-Fc receptor, NA1B-Fc construct and receptor-binding ELISA used in this study has been described previously (Virji *et al*, 1999; Villullas *et al*, 2007).

AUC

Sedimentation equilibrium experiments were performed using a method previously described (Murphy *et al*, 2006). CEACAM1 (0.36 mg/ml) was in 50 mM Hepes (pH 8.0), 150 mM NaCl and UspA1$^{(527-665)}$ (0.13 mg/ml) or CEACAM1/UspA1$^{(527-665)}$ complex (0.07 mg/ml) in 50 mM Tris (pH 8.0) and 150 mM NaCl. In each case, the corresponding buffer was used as a reference. Data were collected at rotor speeds of 10 000, 16 000 and 25 000 r.p.m. after 20 and 24 h by measuring absorbance at 230 or 280 nm, as a function of the radius of centrifugation.

Isothermal titration calorimetry

Complex formation between UspA1$^{(527-665)}$ and N-CEACAM1 was measured using a VP-ITC microcalorimeter (MicroCal) at 37°C. In the first run, UspA1$^{(527-665)}$ at 4 μM in 50 mM Tris–HCl, pH 8.0, 150 mM NaCl, was titrated with a 47 μM solution of N-CEACAM1 in the same buffer in 25 steps of 10 μl; these concentrations were 5 and 100 μM, respectively, in the second run. The raw data were corrected for the competing dimerisation of N-CEACAM1. Data from each of these two runs were analysed using the Origin V5.0 ITC Analysis software assuming a single type of binding and without fixing the number of ligand molecules. The data from the first run gave $N = 2.1 \pm 0.1$ with $K_D = 35 \pm 13$ nM, and in the second run $N = 1.9 \pm 0.1$ and $K_D = 12 \pm 10$.

Structural studies

Determination of the UspA1$^{(527-665)}$ crystal structure, SAXS experiments, molecular modelling and electron microscopy studies were performed using standard methods as described in Supplementary data. X-ray data collection and final refinement statistics are summarised in Table I.

Coordinate deposit

Coordinates and structure factors of the UspA1$^{527-665}$ crystal structure have been deposited with the RCSB Protein Data Bank (accession code 2QIH), and coordinates of the complex are available from www.bris.ac.uk/biochemistry/brady/complexS100.pdb.

Supplementary data

Supplementary data are available at *The EMBO Journal* Online (http://www.embojournal.org).

Acknowledgements

References

Aebi C, Lafontaine ER, Cope LD, Latimer JL, Lumbley SL, McCracken Jr GH, Hansen EJ (1998) Phenotypic effect of isogenic uspA1 and uspA2 mutations on *Moraxella catarrhalis* 035E. *Infect Immun* **66:** 3113–3119

Attia AS, Lafontaine ER, Latimer JL, Aebi C, Syrogiannopoulos GA, Hansen EJ (2005) The UspA2 protein of *Moraxella catarrhalis* is directly involved in the expression of serum resistance. *Infect Immun* **73:** 2400–2410

Bullough PA, Hughson FM, Skehel JJ, Wiley DC (1994) Structure of influenza haemagglutinin at the pH of membrane fusion. *Nature* **371:** 37–43

Cope LD, Lafontaine ER, Slaughter CA, Hasemann Jr CA, Aebi C, Henderson FW, McCracken Jr GH, Hansen EJ (1999) Characterization of the *Moraxella catarrhalis* uspA1 and uspA2 genes and their encoded products. *J Bacteriol* **181:** 4026–4034

Duquerroy S, Vigouroux A, Rottier PJ, Rey FA, Bosch BJ (2005) Central ions and lateral asparagine/glutamine zippers stabilize the post-fusion hairpin conformation of the SARS coronavirus spike glycoprotein. *Virology* **335:** 276–285

Dveksler GS, Dieffenbach CW, Cardellichio CB, McCuaig K, Pensiero MN, Jiang GS, Beauchemin N, Holmes KV (1993) Several members of the mouse carcinoembryonic antigen-related glycoprotein family are functional receptors for the coronavirus mouse hepatitis virus-A59. *J Virol* **67:** 1–8

Fass D, Harrison SC, Kim PS (1996) Retrovirus envelope domain at 1.7 angstrom resolution. *Nat Struct Biol* **3:** 465–469

Fedarovich A, Tomberg J, Nicholas RA, Davies C (2006) Structure of the N-terminal domain of human CEACAM1: binding target of the opacity proteins during invasion of *Neisseria meningitidis* and *N. gonorrhoeae*. *Acta Crystallogr D Biol Crystallogr* **62:** 971–979

Griffiths NJ, Bradley CJ, Heyderman RS, Virji M (2007) IFN-gamma amplifies NFkappaB-dependent *Neisseria meningitidis* invasion of epithelial cells via specific upregulation of CEA-related cell adhesion molecule 1. *Cell Microbiol* **9:** 2968–2983

Guignot J, Peiffer I, Bernet-Camard MF, Lublin DM, Carnoy C, Moseley SL, Servin AL (2000) Recruitment of CD55 and CD66e brush border-associated glycosylphosphatidylinositol-anchored proteins by members of the Afa/Dr diffusely adhering family of

Escherichia coli that infect the human polarized intestinal Caco-2/TC7 cells. *Infect Immun* **68:** 3554–3563

Hammarstrom S (1999) The carcinoembryonic antigen (CEA) family: structures, suggested functions and expression in normal and malignant tissues. *Semin Cancer Biol* **9:** 67–81

Heise T, Dersch P (2006) Identification of a domain in *Yersinia* virulence factor YadA that is crucial for extracellular matrix-specific cell adhesion and uptake. *Proc Natl Acad Sci USA* **103:** 3375–3380

Hill DJ, Edwards AM, Rowe HA, Virji M (2005) Carcinoembryonic antigen-related cell adhesion molecule (CEACAM)-binding recombinant polypeptide confers protection against infection by respiratory and urogenital pathogens. *Mol Microbiol* **55:** 1515–1527

Hill DJ, Virji M (2003) A novel cell-binding mechanism of *Moraxella catarrhalis* ubiquitous surface protein UspA: specific targeting of the N-domain of carcinoembryonic antigen-related cell adhesion molecules by UspA1. *Mol Microbiol* **48:** 117–129

Hoiczyk E, Roggenkamp A, Reichenbecher M, Lupas A, Heesemann J (2000) Structure and sequence analysis of *Yersinia* YadA and *Moraxella* UspAs reveal a novel class of adhesins. *EMBO J* **19:** 5989–5999

Karalus R, Campagnari A (2000) *Moraxella catarrhalis*: a review of an important human mucosal pathogen. *Microbes Infect* **2:** 547

Kegeles G, Rhodes L, Bethune JL (1967) Sedimentation behavior of chemically reacting systems. *Proc Natl Acad Sci USA* **58:** 45–51

Koretke KK, Szczesny P, Gruber M, Lupas AN (2006) Model structure of the prototypical non-fimbrial adhesin YadA of *Yersinia enterocolitica*. *J Struct Biol* **155:** 154

Korotkova N, Yang Y, Le Trong I, Cota E, Demeler B, Marchant J, Thomas WE, Stenkamp RE, Moseley SL, Matthews S (2008) Binding of Dr adhesins of *Escherichia coli* to carcinoembryonic antigen triggers receptor dissociation. *Mol Microbiol* **67:** 420–434

Lafontaine ER, Cope LD, Aebi C, Latimer JL, McCracken Jr GH, Hansen EJ (2000) The UspA1 protein and a second type of UspA2 protein mediate adherence of *Moraxella catarrhalis* to human epithelial cells *in vitro*. *J Bacteriol* **182:** 1364–1373

Leusch HG, Drzeniek Z, Markos-Pusztai Z, Wagener C (1991) Binding of *Escherichia coli* and *Salmonella* strains to members of the carcinoembryonic antigen family: differential binding inhibition by aromatic alpha-glycosides of mannose. *Infect Immun* **59:** 2051–2057

Linke D, Riess T, Autenrieth IB, Lupas A, Kempf VA (2006) Trimeric autotransporter adhesins: variable structure, common function. *Trends Microbiol* **14:** 264–270

Lovell SC, Davis IW, Arendall III WB, de Bakker PI, Word JM, Prisant MG, Richardson JS, Richardson DC (2003) Structure validation by Calpha geometry: phi, psi and Cbeta deviation. *Proteins* **50:** 437–450

Lupas A (1996) Coiled coils: new structures and new functions. *Trends Biochem Sci* **21:** 375–382

Meehan M, Kelly SM, Price NC, Owen P (2002) The C-terminal portion of the fibrinogen-binding protein of *Streptococcus equi* subsp. *equi* contains extensive alpha-helical coiled-coil structure and contributes to thermal stability. *FEMS Microbiol Lett* **206:** 81–86

Meng G, Surana NK, St Geme III JW, Waksman G (2006) Structure of the outer membrane translocator domain of the *Haemophilus influenzae* Hia trimeric autotransporter. *EMBO J* **25:** 2297–2304

Murphy TA, Catto LE, Halford SE, Hadfield AT, Minor W, Walsh TR, Spencer J (2006) Crystal structure of *Pseudomonas aeruginosa* SPM-1 provides insights into variable zinc affinity of metallo-beta-lactamases. *J Mol Biol* **357:** 890–903

Nordstrom T, Blom AM, Forsgren A, Riesbeck K (2004) The emerging pathogen *Moraxella catarrhalis* interacts with complement inhibitor C4b binding protein through ubiquitous surface proteins A1 and A2. *J Immunol* **173:** 4598–4606

Nummelin H, Merckel MC, Leo JC, Lankinen H, Skurnik M, Goldman A (2004) The *Yersinia* adhesin YadA collagen-binding domain structure is a novel left-handed parallel beta-roll. *EMBO J* **23:** 701–711

Oomen CJ, van Ulsen P, van Gelder P, Feijen M, Tommassen J, Gros P (2004) Structure of the translocator domain of a bacterial autotransporter. *EMBO J* **23:** 1257–1266

Petoukhov MV, Svergun DI (2005) Global rigid body modeling of macromolecular complexes against small-angle scattering data. *Biophys J* **89:** 1237–1250

Ruiz T, Lenox C, Radermacher M, Mintz KP (2006) Novel surface structures are associated with the adhesion of *Actinobacillus actinomycetemcomitans* to collagen. *Infect Immun* **74:** 6163–6170

Sheriff S, Chang CY, Ezekowitz RA (1994) Human mannose-binding protein carbohydrate recognition domain trimerizes through a triple alpha-helical coiled-coil. *Nat Struct Biol* **1:** 789–794

Svergun D, Barberato C, Koch MHJ (1995) CRYSOL—a program to evaluate X-ray solution scattering of biological macromolecules from atomic coordinates. *J Appl Crystallogr* **28:** 768–773

Svergun DI (1999) Restoring low resolution structure of biological macromolecules from solution scattering using simulated annealing. *Biophys J* **76:** 2879–2886

Tan TT, Forsgren A, Riesbeck K (2006) The respiratory pathogen *Moraxella catarrhalis* binds to laminin via ubiquitous surface proteins A1 and A2. *J Infect Dis* **194:** 493–497

Tan TT, Nordstrom T, Forsgren A, Riesbeck K (2005) The respiratory pathogen *Moraxella catarrhalis* adheres to epithelial cells by interacting with fibronectin through ubiquitous surface proteins A1 and A2. *J Infect Dis* **192:** 1029–1038

Tao Y, Strelkov SV, Mesyanzhinov VV, Rossmann MG (1997) Structure of bacteriophage T4 fibritin: a segmented coiled coil and the role of the C-terminal domain. *Structure* **5:** 789–798

Villullas S, Hill DJ, Sessions RB, Rea J, Virji M (2007) Mutational analysis of human CEACAM1: the potential of receptor polymorphism in increasing host susceptibility to bacterial infection. *Cell Microbiol* **9:** 329–346

Virji M, Evans D, Hadfield A, Grunert F, Teixeira AM, Watt SM (1999) Critical determinants of host receptor targeting by *Neisseria meningitidis* and *Neisseria gonorrhoeae*: identification of Opa adhesiotopes on the N-domain of CD66 molecules. *Mol Microbiol* **34:** 538–551

Virji M, Watt SM, Barker S, Makepeace K, Doyonnas R (1996) The N-domain of the human CD66a adhesion molecule is a target for Opa proteins of *Neisseria meningitidis* and *Neisseria gonorrhoeae*. *Mol Microbiol* **22:** 929–939

Volkov VV, Svergun DI (2003) Uniqueness of *ab initio* shape determination in small-angle scattering. *J Appl Crystallogr* **36:** 860–864

Walshaw J, Woolfson DN (2001) Socket: a program for identifying and analysing coiled-coil motifs within protein structures. *J Mol Biol* **307:** 1427–1450

Watt SM, Teixeira AM, Zhou GQ, Doyonnas R, Zhang Y, Grunert F, Blumberg RS, Kuroki M, Skubitz KM, Bates PA (2001) Homophilic adhesion of human CEACAM1 involves N-terminal domain interactions: structural analysis of the binding site. *Blood* **98:** 1469–1479

Wilson IA, Skehel JJ, Wiley DC (1981) Structure of the haemagglutinin membrane glycoprotein of influenza virus at 3 Å resolution. *Nature* **289:** 366–373

Wollmann P, Zeth K, Lupas AN, Linke D (2006) Purification of the YadA membrane anchor for secondary structure analysis and crystallization. *Int J Biol Macromol* **39:** 3–9

Wu H, Kwong PD, Hendrickson WA (1997) Dimeric association and segmental variability in the structure of human CD4. *Nature* **387:** 527–530

Yeo HJ, Cotter SE, Laarmann S, Juehne T, St Geme III JW, Waksman G (2004) Structural basis for host recognition by the *Haemophilus influenzae* Hia autotransporter. *EMBO J* **23:** 1245–1256